Progress toward larger molecular simulation on a quantum computer: Simulating a system with up to 28 qubits accelerated by point-group symmetry

Changsu Cao,[1,2] Jiaqi Hu [●],[3] Wengang Zhang,[1,3,4] Xusheng Xu [●],[1] Dechin Chen [●],[1] Fan Yu,[1] Jun Li,[2,5] Han-Shi Hu [●],[2,*] Dingshun Lv [●],[1,†] and Man-Hong Yung[1,3,4,‡]

[1]*Central Research Institute, 2012 Labs, Huawei Technologies, Shenzhen, 518129, China*
[2]*Department of Chemistry, Tsinghua University, Beijing 100084, China*
[3]*Department of Physics, Southern University of Science and Technology, Shenzhen 518055, China*
[4]*Shenzhen Institute for Quantum Science and Engineering, Southern University of Science and Technology, Shenzhen 518055, China*
[5]*Department of Chemistry, Southern University of Science and Technology, Shenzhen 518055, China*

The exact evaluation of the molecular ground state in quantum chemistry requires an exponentially increasing computational cost. Quantum computation is a promising way to overcome the exponential problem using polynomial-time quantum algorithms. A quantum-classical hybrid optimization scheme known as the variational quantum eigensolver is preferred for noisy intermediate-scale quantum devices. However, the circuit depth becomes one of the bottlenecks of its application to large molecules of more than 20 qubits. In this work, we employ point-group symmetry to reduce the number of operators in constructing ansatz so as to achieve a more compact quantum circuit. We illustrate this methodology with a series of molecules ranging from LiH (12 qubits) to C_2H_4 (28 qubits). A significant reduction of up to 82% of the operator numbers is reached on C_2H_4. This also sheds light onto further work in this direction to construct even shallower ansatz with enough expressive power and simulate even larger scale systems.

I. INTRODUCTION

Quantum computing is proposed to be a promising way to overcome the exponential issue in simulating the energies and properties of the many-electron molecular system by classical computers, as speculated by Feynman in 1982 [1]. Since then, various quantum algorithms have been developed [2–8], among which, the variational quantum eigensolver (VQE) [8–12] is believed to be friendly to near-term quantum devices for its noise-resilient property and its small need for quantum gates, which is a benefit of its hybrid quantum-classical framework [13].

The VQE has been applied to simulate chemical systems both experimentally and numerically. The first demonstration of H_2 (2 qubits) on quantum devices was presented in Ref. [8]. After that, a variety of quantum simulations were performed for BeH_2 (6 qubits) [11], H_2O (8 qubits) [14], and H_{12} (12 qubits) [15].

To benchmark the performance or optimize the algorithm, the numerical results are also presented using virtual quantum simulators on different molecules [16–18]. To date, the largest is 20 qubits for H_2O [17] with 6-31G basis set.

The scale of the simulation is limited by two correlated factors, the number of controllable qubits and the circuit depth. Although the top record of the controllable qubit number

reached 66 [19], the depth of the quantum circuit is still a problematic limitation on large-scale quantum chemical simulation. Therefore, to extend the scale of quantum chemical simulation, a better ansatz initialization requires not only smaller demand for qubit number but also using less parameters for a more compact quantum circuit.

The unitary coupled-cluster (UCC) ansatz was used when VQE was initially proposed, and has been one of the most popular choices since then. In order to represent the molecule with less parameters for a more compact quantum circuit, one feasible method is to screen out the less important parameters based on UCC ansatz by precalculations or using adaptive methods [20–23]. Different improved coupled-cluster (CC) ansatzes are also proposed and reached hopeful results [24–27].

Besides these methods, for the chemical system, using the intrinsic information of it might be of more benefit to obtain the compact ansatz and introduce less approximations.

For example, the particle number conservation (U(1) symmetry) and the fermionic parity conservation (Z_2 symmetry) are used as restrictions in VQE [28–30]. The geometric property of molecules described by the point-group symmetry will also provide great convenience for quantum chemical simulation, for which the power has already been demonstrated in conventional *ab initio* chemical calculations in classical computers [31–33]. However, the power of point-group symmetry is rarely explored in the quantum computing regime. Currently, point-group symmetry has been used for two purposes: removing qubits in simulation [34,35] and reducing the depth of quantum circuits in quantum computing [36,37].

*[*]hshu@mail.tsinghua.edu.cn
*[†]*ywlds@163.com
*[‡]*yung.manhong@huawei.com

Setia *et al.* reduced the qubits in simulation by using the point group to find the permutation matrix to do qubit tapering off [34]. Fischer and Gunlycke mapped the configuration states based on point-group symmetry to qubits rather than the molecular orbitals, which makes it possible to represent the same molecule with less qubits [35]. By applying projectors of symmetry operators to the prepared quantum state, the depth of the quantum circuit can be reduced at the cost of more measurements [36,37].

In this work, we use point-group symmetry to directly reduce the operator numbers in the UCC ansatz so that the depth of the quantum circuit is significantly decreased without damage to the accuracy or expensive auxiliary calculations. We present a series of numerical cases with the symmetry-reduced unitary coupled-cluster singles and doubles (SymUCCSD) ansatz by the MindQuantum simulator, including LiH, HF, H_2O, BeH_2, CH_4, and NH_3 with its flipping potential energy surface. We have also successfully performed the simulation of 28-qubit C_2H_4 on the virtual quantum simulator.

II. FRAMEWORK

The VQE method was originally designed to solve the ground-state energies of a molecular Hamiltonian [9]. Typically, in these problems, the Hamiltonian under Born-Oppenheimer approximation is usually written in a second-quantized form [5] as

$$\hat{H} = \sum_{p,q} h_{pq} \hat{a}_p^\dagger \hat{a}_q + \frac{1}{2} \sum_{p,q,r,s} g_{pqrs} \hat{a}_p^\dagger \hat{a}_r^\dagger \hat{a}_s \hat{a}_q, \qquad (1)$$

where $\hat{a}_p^\dagger$ and $\hat{a}_p$ denote the fermionic creation operator and annihilation operator associated with the pth fermionic mode (or spin orbital). The sets of coefficients $\{h_{pq}\}$ and $\{g_{pqrs}\}$ are called one- and two-electron integrals and can be evaluated by classical computers. The main idea of VQE is that the parametrized quantum state $\Psi(\vec{\theta})$ is prepared and measured on a quantum computer, while the parameters are updated in a classical computer following the variational principle $E_0 \leqslant \min_{\vec{\theta}} \langle \Psi(\vec{\theta}) | \hat{H} | \Psi(\vec{\theta}) \rangle$, where E_0 is the ground-state energy.

The essential part for VQE is to construct the parametrized quantum state $\Psi(\vec{\theta})$ that is close enough to the unknown ground state. The ansatz derived from the UCC method [5,38–41] is one of the most popular choices. $\Psi(\vec{\theta})$ can be constructed as

$$|\Psi(\vec{\theta})\rangle = e^{\hat{T}(\vec{\theta}) - \hat{T}^\dagger(\vec{\theta})} |\Psi_0\rangle, \qquad (2)$$

where $\hat{T}$ are the coupled-cluster excitations, and $|\Psi_0\rangle$ is the initial state (usually a Hartree-Fock state). The coupled-cluster excitations are usually truncated to single and double excitations, named UCCSD:

$$\hat{T}_1(\boldsymbol{\theta}) = \sum_{i,a} \hat{t}_i^a = \sum_{i,a} \theta_i^a \hat{a}_a^\dagger \hat{a}_i, \qquad (3)$$

$$\hat{T}_2(\boldsymbol{\theta}) = \sum_{i,j,a,b} \hat{t}_{ij}^{ab} = \sum_{i,j,a,b} \theta_{ij}^{ab} \hat{a}_a^\dagger \hat{a}_b^\dagger \hat{a}_i \hat{a}_j. \qquad (4)$$

To implement the VQE circuit of the UCC ansatz on a quantum device, the Trotter-Suzuki expansion is needed. Conventionally, the first-order Trotterization is enough to reproduce UCCSD results, while more Trotter steps hardly

---

Algorithm 1 Scheme of SymUCCSD in VQE

1. Initialize the reference state $|\Psi_0\rangle$ (usually the Hartree-Fock ground state).
2. **For** each possible excitation operator $\hat{t}$ in $\hat{T}$
    If $D(e^{\hat{t}-\hat{t}^\dagger} |\Psi_0\rangle) \neq D(|\Psi_0\rangle)$
      Remove $\hat{t}$ from $\hat{T}$.
    End
End
3. Construct the ansatz operator $e^{\hat{T}-\hat{T}^\dagger}$ by the reduced $\hat{T}$.
4. Convert the ansatz operator to the quantum circuit and prepare the ansatz.
5. Perform VQE loop with the generated ansatz until the energy converges or reaches the maximum number of iterations.

---

improve the accuracy but significantly elongate quantum circuit depth [13,42]. The UCCSD ansatz with first-order Trotterization is expressed as

$$|\Psi(\vec{\theta})\rangle_{\text{Trot}} = \prod_{i,a} e^{\hat{t}_i^a - \hat{t}_i^{a\dagger}} \prod_{i,j,a,b} e^{\hat{t}_{ij}^{ab} - \hat{t}_{ij}^{ab\dagger}} |\Psi_0\rangle. \qquad (5)$$

For this chemical-inspired ansatz, it is natural to utilize the built-in information of the molecule to reduce the computational cost. According to the point group, the symmetric properties of the molecular wavefunction can be described by the irreducible representation (irrep). The point-group symmetry has been employed in classic quantum chemical calculations as a common practice. In CC theory, the amplitude of the excitation operator will vanish unless the corresponding term preserves the totally symmetric irrep, which has been shown by Čá *et al.* [31] and by Stanon *et al.* [32]. In UCC theory, however, the introduction of the deexcitation operator $\hat{t}^\dagger$ prevents natural truncation and the operator terms cannot be expressed with finite terms as it is in CC theory. The previous conclusion in CC theory cannot directly apply in UCC theory and it is not trivial whether the symmetry constraint is still valid. We provide a detailed derivation in Appendix B that the constraint still holds. In this sense, only the excitation that belongs to the same irrep of the reference state is valid in the UCC ansatz:

$$\forall D(e^{\hat{t}-\hat{t}^\dagger} |\Psi_0\rangle) \neq D(|\Psi_0\rangle) : e^{\hat{t}-\hat{t}^\dagger} = 1, \qquad (6)$$

where D is the irrep of the corresponding wavefunction.

The key step of our method is to compare the irrep of all the possible excited states with the reference state. The wavefunction is expressed as the Slater determinant of a collection of molecular orbitals, i.e., $|\Psi_0\rangle = |\phi_1 \bar{\phi}_1 \phi_2 \bar{\phi}_2 \cdots \phi_n \bar{\phi}_n\rangle$, where ϕ is the occupied molecular spin orbital and the bar indicates the different spin. The irrep of each molecular orbital can be determined automatically after the Hartree-Fock calculation on classic computers by most of quantum chemical packages like PySCF [43,44]. Accordingly, the irrep of the excited state (and operator) is determined from the direct product of the irrep of the molecular spin orbitals by looking up the product table of irreps, which needs no complex numerical computations.

The overallflow can be summarized in Algorithm 1 and we term this the SymUCCSD method in the following of this work.
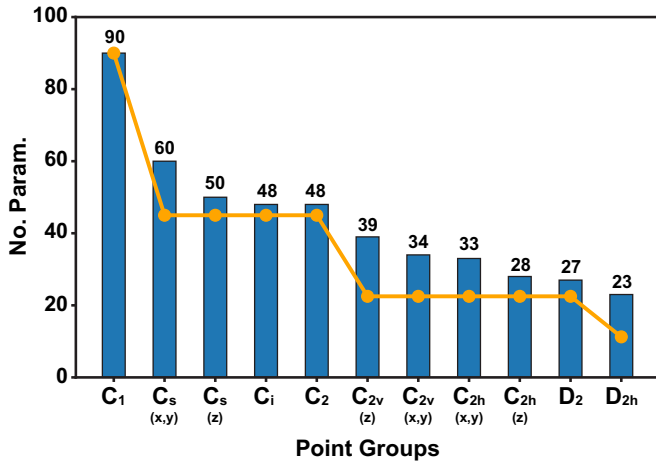
FIG. 1. Parameter reduction of BeH_2 under various point groups. The orientation of the symmetry elements changes the ratio of reduction slightly. The orange line is the hypothetical situation that the number of configurations belonging to each irrep is equal.

III. NUMERICAL RESULTS

Using the symmetry-reduction method mentioned above, we performed the symmetry-reduced UCCSD-VQE on several testing systems, varying from 12 qubits for LiH to 28 qubits for C_2H_4. Specially, we simulated BeH_2 under various point-group symmetries to study the relationship between the order of the group and the reduction of parameters. The flipping of ammonia, which involves the nonequilibrium geometry structures, was simulated as well. All the VQE simulations are performed using the quantum simulator MindQuantum [45]. The STO-3G basis set was employed in all cases [46]. The fermion operators are transformed to qubit-type operators by Jordan-Wigner transformation [47]. The gradient-based optimization method Broyden-Fletcher-Goldfarb-Shanno (BFGS) is used to minimize the energy expectation value generated by MindQuantum, of which the convergence threshold is 10^{-6}. All the geometric structures are obtained from the computational chemistry comparison and benchmark database (CCCBDB)-NIST Database [48].

A. BeH_2: Under different point-group symmetries

A specific molecule belongs to different point groups, i.e., the point group with the highest symmetry and its subgroups. Here we simulate BeH_2 with various point groups assigned to it to investigate the relationship between the order of the group and the reduction of the ansatz. D_{2h} is the highest-order Abelian point group that BeH_2 belongs to. Alternatively, the subgroup of D_{2h}, i.e., D_2, C_{2h}, C_{2v}, C_2, C_s, C_i, and C_1, can also been employed to reduce the ansatz in Sec. II. We display the number of remaining parameters in Fig. 1, which is approximately proportional to the reciprocal of the order of the group, $1/h$. The reference line of $1/h$ is also depicted.

The C_1 group, which is composed of the identity operation exclusively, has only the A irrep and means "no symmetry." Thus SymUCCSD here works exactly as the original UCCSD-VQE calculation. The second-order groups C_s, C_i, and C_2 include an additional single reflection (mirror plane),

inversion (inversion center), or single rotation (rotation axis) operation, respectively. Around half of the parameters are filtered out when employing the second-order groups while the orientation of symmetry elements will affect the efficiency of the reduction. Similarly, the number of parameters is further reduced when applying the fourth-order groups, C_{2v}, C_{2h}, and D_2, and the eighth-order group, D_{2h}. The promotion in parameter reduction becomes small from the fourth-order groups to the eighth-order group D_{2h}.

In our method, only parameters belonging to the referenced irrep would survive. The order of the group equals the number of irreps, which explains the $1/h$ reduction ratio. The excited terms may distribute unevenly in each irrep especially in small systems. The uneven distribution problem will be improved when it comes to larger systems as we will find below.

B. Simulations of small molecules

A variety of molecules, i.e., the hydrides containing the second-row elements, are chosen as the testing cases for the benchmark, including LiH, HF, H_2O, BeH_2, NH_3, and CH_4. In SymUCCSD calculations, the highest possible Abelian point group was chosen to simplify the ansatz. Among the testing molecules, the ratio of the remaining parameters ranges from 26% in BeH_2 with D_{2h} to 56% in NH_3 with C_s. In the worst case that we tested, around half of the parameters are reduced as the lower bound for the symmetric molecular systems, corresponding to half the size of the quantum circuit. As shown in Table I, the energy calculated by SymUCCSD, UCCSD, and coupled-cluster singles and doubles (CCSD) results is compared to the reference energies computed by the exact solution of full configuration interaction (FCI). The errors are all less than 1.6 mhartree (chemical accuracy at the level of STO-3G). Furthermore, the difference of computed energy between UCCSD without parameter reduction and SymUCCSD is even a few orders of magnitude smaller. The worst case is no more than 0.005 mhartree, approaching the threshold of computational convergence. The energy difference between UCCSD and SymUCCSD are within the convergence threshold, indicating that the method actually filters out some redundant parameters without harm to the accuracy.

Note that we also performed numerical simulations of adaptive derivative-assembled pseudo-trotter ansatz variational quantum eigensolver (ADAPT-VQE) [20], as a comparison and combination with SymUCCSD on BeH_2. The results show that ADAPT-VQE can efficiently save measurement cost by combining with SymUCCSD, and the operators selected in ADAPT-VQE indeed satisfied the point-group-symmetry constraint. For further details, we refer the reader to Appendix D.

To evaluate the performance on real quantum computers, we have compared SymUCCSD with conventional UCCSD on H_4 with depolarizing noise and limited measurement shots. According to our numerical results in Appendix E, SymUCCSD is more robust and accurate than UCCSD.

So removing the unfavored operators in the UCCSD ansatz will not sacrifice the accuracy of the result, as supported by Appendix B that the cluster operator should be totally symmetric and not change the symmetry of the reference

TABLE I. VQE simulations for small molecules. The simulation scale ranges from 12 to 18 qubits. The original parameters and the parameters after reduction are shown in the fourth and fifth columns. The percentage of parameters used of the symmetry reduction ansatz compared to the original UCCSD ansatz is shown in the sixth column. The energy differences compared with the FCI energy are shown from seventh to ninth columns with units in hartree. The last column displays the energy difference between UCC and SymUCC. The equilibrium geometric structures of these molecules are obtained from the CCCBDB-NIST Database [48].

	Qubits	Sym.	Parameters before	Parameters after	%	ΔE_{CCSD}	ΔE_{UCCSD}	$\Delta E_{SymUCCSD}$	$\Delta E_{UCC-SymUCC}$
HF	12	C_{2v}	20	11	55%	2.94×10^{-8}	1.82×10^{-5}	1.38×10^{-5}	4.39×10^{-6}
LiH	12	C_{2v}	44	20	45%	1.05×10^{-5}	1.10×10^{-5}	1.09×10^{-5}	1.08×10^{-7}
H_2O	14	C_{2v}	65	26	40%	1.17×10^{-4}	1.19×10^{-4}	1.09×10^{-4}	9.96×10^{-6}
BeH_2	14	D_{2h}	90	23	26%	3.94×10^{-4}	3.83×10^{-4}	3.82×10^{-4}	8.89×10^{-7}
NH_3	16	C_s	135	75	56%	2.14×10^{-4}	1.94×10^{-4}	1.86×10^{-4}	8.44×10^{-6}
CH_4	18	D_2	230	65	28%	2.30×10^{-4}	2.06×10^{-4}	1.96×10^{-4}	9.94×10^{-6}

wavefunction; otherwise the generated coupled-cluster wavefunction would not be the eigenvector of the Hamiltonian.

C. Ammonia flipping

The molecule in the nonequilibrium geometry is important when studying the chemical reaction process which involves bond breaking and conformations changes. To explore the scenario of the nonequilibrium structures, we choose the ammonia flipping process to demonstrate our algorithm. The reaction coordination is computed using a Perdew-Burke-Ernzerhof (PBE) density functional approximation [49] with def2-TZVP [50] basis set in PySCF [43,44]. The energy profiles regarding FCI, CCSD, and SymUCCSD methods are shown in Fig. 2. Concerning the flipping process, the C_s symmetry is kept so that the parameter reduction is the same as that in Table I.

When referring to the FCI results, the error increases when the structure turns from equilibrium to nonequilibrium geometries and reaches the maximum at the flat structure ($\angle z$-N-H $= 90°$), 0.35 mhartree for CCSD and 0.33 mhartree for SymUCCSD. It agrees with our intuition that in the nonequilibrium structure, the multireference properties are not negligible anymore. FCI describes the multireference properties well, while the truncated CCSD and UCCSD are generally believed to be single-reference methods. The energies calculated by SymUCCSD are slightly lower than those by CCSD. It is probably attributed to the introducing of the deexcitation operator in the UCC ansatz.

D. C_2H_4: Large molecule simulation

Simulations with more qubits (indicating more orbitals in the molecule) usually require more parameters and deeper quantum circuits. If we can construct a more compact ansatz, larger molecular simulations will become tractable under the current quantum resource. To explore the boundary of our method in the current simulator, we present a simulation on a 28-qubit C_2H_4 molecule. As shown in Fig. 3, the calculation converges after 25 iterations and reaches the chemical accuracy at the level of STO-3G around the 12th iteration. The geometric structure of C_2H_4 belongs to the D_{2h} point group. The symmetry of the total wavefunction is A_g irrep. Table II shows that there are 48 single excitations and 1176 double excitations distributing in various irreps. Only 18% of the parameters belonging to A_g remain after the symmetry

reduction, which significantly shortens the depth of the circuit. The greatly reduced number of parameters is an important reason that makes such a simulation tractable with the current quantum simulator.

IV. CONCLUSION

In this work, we have presented an algorithm to reduce the number of operators needed in the UCCSD ansatz by
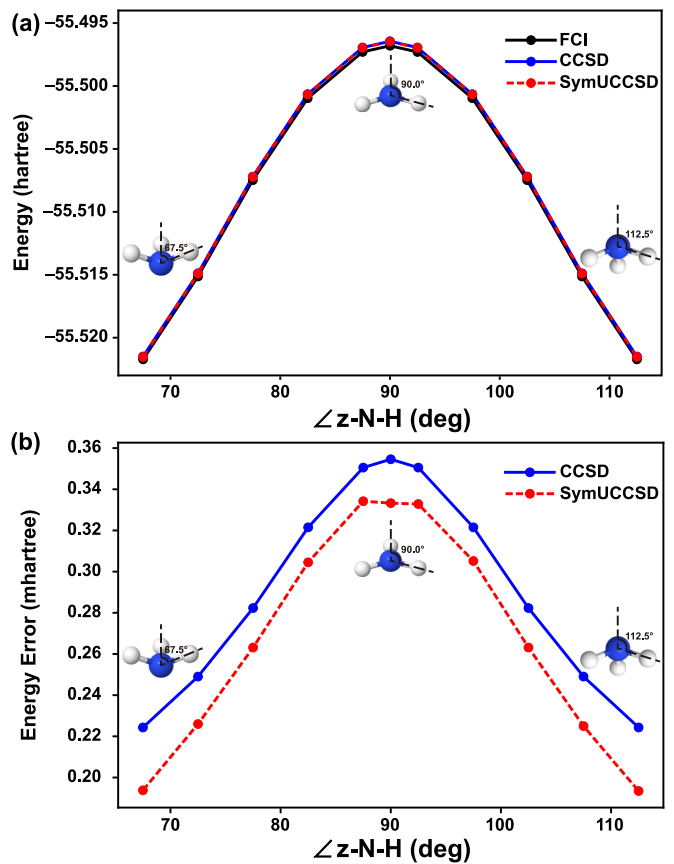

FIG. 2. The potential energy curve of the ammonia flipping. (a) Potential energy surface calculated by FCI, CCSD, and the symmetry-reduced UCCSD during ammonia flipping. (b) Energy deviation compared with FCI energy. The flipping process is described by the angle of the z axis, N atom, and H atom. The unit of the error is millihartree.
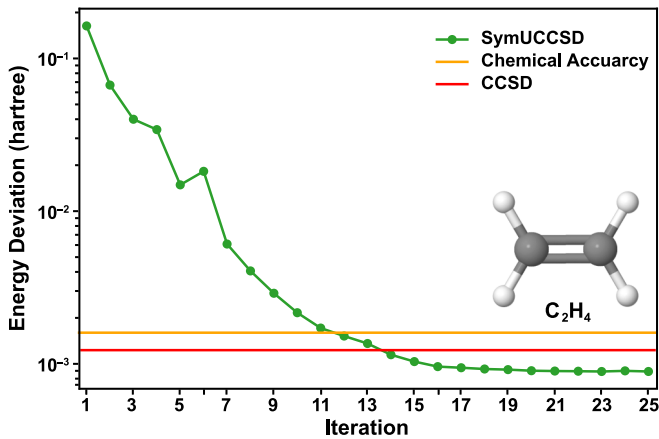
FIG. 3. The convergence process of SymUCCSD for C_2H_4. The green line denotes the energy deviation of SymUCCSD compared to FCI energy vs iteration numbers. The orange line denotes the energy deviation derived from CCSD vs FCI and the green line indicates chemical at the level of STO-3G with reference to FCI results (0.0016 hartree).

employing point-group symmetry. The detailed derivation of this method is given in Appendix B. After testing various molecules in different point groups using this method implemented in the MindQuantum simulator [45], we observed that the reduction rate is approximately proportional to $1/h$, where h is the rank of the group. Molecules with higher symmetry such as D_{2h} could lead to a larger reduction of the number of operators, meaning more compact quantum circuits. With the help of this scheme, we successfully simulated a 28-qubit C_2H_4 molecule in a reasonable computing resource. We note that with a supercomputer we can simulate an even larger molecular system. The importance of this large-scale simulation also lies in that, at this level, the UCCSD ansatz is a good ansatz with enough expressive power [51,52]. This also sheds light on the further work in this direction to construct an even shallower ansatz and simulate an even larger scale system.

In principle, point-group symmetry is valid and nonexclusive for arbitrary molecular systems using the UCC ansatz. It is proposed to be compatible with other methods based on excitation operators to compress further the quantum circuit depth, such as low-rank decomposition and low depth circuits [6,53–56], (fermion or qubit) ADAPT-VQE, or k-UpCCGSD

TABLE II. The number of the excited configurations belonging to each irrep for C_2H_4.

Irrep	No. of excitations, T_1	No. of excitations, T_2
A_g	9	210
B_{1g}	8	176
B_{2g}	2	104
B_{3g}	5	110
A_u	2	104
B_{1u}	3	114
B_{2u}	11	182
B_{3u}	8	176
Total	48	1176

[22]. It is proposed to be compatible with other methods based on excitation operators to compress further the quantum circuit depth, such as the energy sorting scheme [22], (fermion or qubit) adapt VQE proposed in Refs. [20,57,58], or k products of the exponential of pair unitary coupled-cluster double-excitation operators together with generalized single-excitation operators (k-UpCCGSD) [27]. Besides such algorithms inspired by the problems to reduce the quantum circuit depth, the quantum circuit compilation [59,60] is also very important and inevitable to implement simulations of the molecule with chemical interests on real quantum hardware, such as superconducting or trapped-ion systems.

To further enable even larger scale or more realistic chemistry simulations [61], the current scheme may be incorporated by treating the current method as a module and incorporating it into the deep VQE method [62,63], the virtual quantum subspace expansion method [64], the quantum hybrid tensor network [65], and the quantum embedding methods [66–73].

With the advancement of the aforementioned algorithms and the progress in quantum hardware, we anticipate a solid step towards the simulation of realistic molecular systems on the quantum computer soon.

APPENDIX A: POINT GROUP

In this section we briefly introduce the relevant knowledge of point groups. For a more detailed and systematic introduction of point groups please refer to Refs. [74–76]. The point group is a set of symmetry operations under which the object is indistinguishable from the original geometry. In this paper, we mainly refer the object as a molecule. The so-called point group comes from the origin point being unchanged with arbitrary symmetry operation since all the symmetry elements intersect at it. The symmetry operations include reflection, inversion, rotation, and identity operation, which correspond to symmetry elements of mirror planes σ, inversion center i, rotation axes C_n, and identities E, respectively. A molecule belongs to a symmetry point group if it is unchanged under all the symmetry operations of this group.

In application, the character table and the product table are the essential and frequently used devices for the point group. Figure 4 is a typical character table of the D_{2h} group, in which the rows are the irreducible group representations and the columns are the conjugacy class of the symmetric operations. The table entries are the characters (trace of the matrix) of the symmetric operations under the different irreducible representations. Figure 5(a) is the product table of the D_{2h} group, which exhibits how the character changes under the direct product of the representations. Since the characters of the representation of a direct product are equal to the products of the characters of the representations based on the individual sets of functions, the product table of the point group can be generated by the products of the characters.

D_{2h}	E	$C_2(x)$	$C_2(y)$	$C_2(z)$	i	$\sigma(xy)$	$\sigma(xz)$	$\sigma(yz)$
A_g	1	1	1	1	1	1	1	1
B_{1g}	1	-1	-1	1	1	1	-1	-1
B_{2g}	1	-1	1	-1	1	-1	1	-1
B_{3g}	1	1	-1	-1	1	-1	-1	1
A_u	1	1	1	1	1	-1	-1	-1
B_{1u}	1	-1	-1	1	1	-1	1	1
B_{2u}	1	-1	1	-1	1	1	-1	1
B_{3u}	1	1	-1	-1	1	1	1	-1

FIG. 4. The character table of the D_{2h} group for BeH_2.

Taking the direct product of B_{1g} and B_{2g} as an example, the characters of B_{1g} are 1, -1, -1, 1, 1, 1, -1, -1 and those of B_{2g} are 1, -1, 1, -1, 1, -1, 1, -1. The products of the characters under each conjugacy class of the group element are 1, 1, -1, -1, 1, -1, -1, 1, respectively, which correspond to the characters of B_{3g} irreducible representation. So the direct product of B_{1g} and B_{2g} leads to B_{3g}. Similarly, a product table of the D_{2h} group is constructed according to the result of the direct product between two arbitrary irreps.
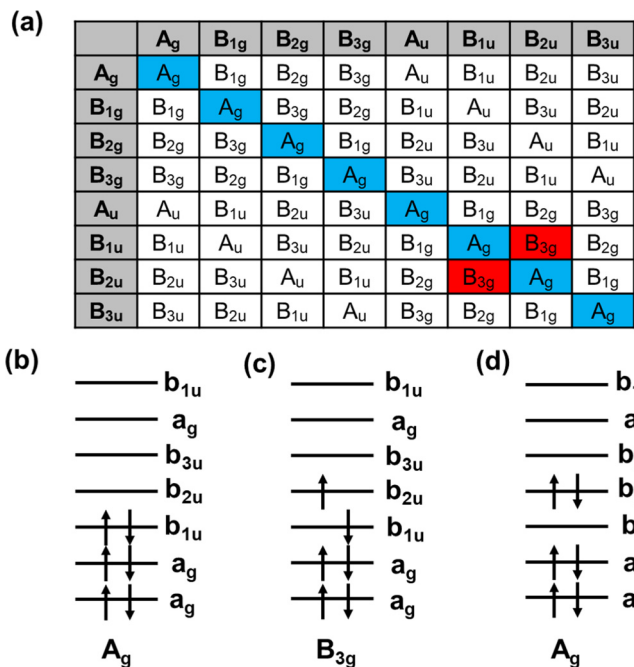
FIG. 5. The irrep of the D_{2h} point group for a BeH_2 molecule. (a) The product table for the irreducible representations of the D_{2h} group. (b) The electron configuration diagram of BeH_2 of the reference state, i.e., the Hartree-Fock state with irrep A_g. (c) An example of coupled-cluster terms that correspond to a configuration with different irrep B_{3g} compares to the reference state. This term is a single excitation concerning the reference term. (d) An example of coupled-cluster terms that correspond to a configuration with the same irrep A_g as the reference state. Note that it is conventional to label the irrep of the molecular orbital in lower case like a_g and the irrep of the molecular state in upper case like A_g.
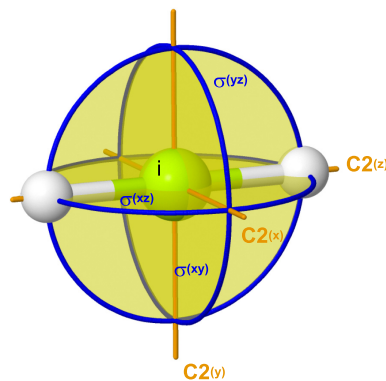
FIG. 6. The symmetry elements of BeH_2 in the D_{2h} point group. Rotation axes C_2, reflection mirrors σ, and inversion center i are depicted in the figure.

Here we take BeH_2 as an example to illustrate detailed steps for our algorithm. The BeH_2 structure belongs to the $D_{\infty h}$ group, which is non-Abelian. In this paper, we only discuss the Abelian situation which is easy to handle. Here, we take the D_{2h} group, an Abelian subgroup of $D_{\infty h}$ with the highest rank, to reduce the parameters of BeH_2. The Cartesian coordinate system is set up with the origin at the Be atom and the z axis along Be-H as shown in Fig. 6.

There are eight symmetry operations corresponding to the same number of symmetry elements for BeH_2 under the D_{2h} group. Three C_2 rotation axes are along the x, y, and z axes, and three mirrors are in the xy, yz, and zx planes which are perpendicular with each other and intersect in a C_2 rotation axis. The rest of the symmetry elements are the inversion center at the location of the Be atom and the identity. We display molecular orbitals of BeH_2 to illustrate how to understand the spatial symmetry in it combining with the character table. The isosurfaces of molecular orbitals are depicted in Fig. 7, in which the blue surface represents the positive value, and the red surface represents the negative one. The character in Fig. 4 indicates how the sign of the certain irreducible representation changes under the particular symmetry operation. For the A_g orbitals, the sign of the wavefunction is maintained under arbitrary symmetry operation. Thus, all the characters are 1. For the B_{1u} orbitals like orbital 3 and orbital 7, the sign of the wavefunction is kept after rotating along the z axis or reflected by the xz and yz planes. But the sign changes after rotation by x axis and y axis or reflection by xy plane. Thus, the characters
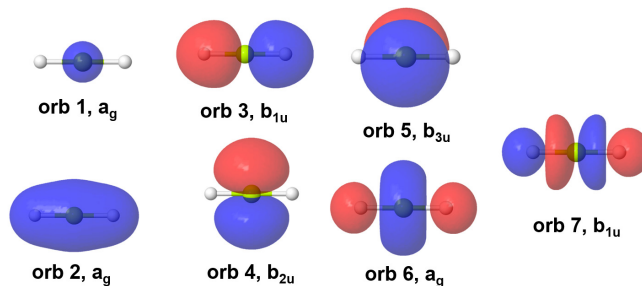
FIG. 7. The isosurface of the wavefunction of the molecular orbital. (Isovalue is 0.03 arbitrary units.)

are -1 for i, $C_2(x)$, $C_2(y)$, and $\sigma(xy)$ and $+1$ for the other operations. The product table is then generated according to the character table as shown in Fig. 5(a). Then it is possible to get the irrep of the excited term. The key step is to determine the irrep of the excited terms (or the excitation operators) and retain only the appropriate items by referring to the product table. The wavefunction of the reference state is expressed as the Slater determinant of a collection of molecular orbitals, i.e., $|\Psi_0\rangle = |\phi_1\overline{\phi}_1\phi_2\overline{\phi}_2\cdots\phi_n\overline{\phi}_n\rangle$, where ϕ is the occupied molecular spin orbital and the bar indicates the different spin. The irrep of the molecular state is determined from the direct product of the molecular spin orbitals.

Again we go back to BeH$_2$ in the D_{2h} point group. In Fig. 5(a) we provide a product table for the D_{2h} group, where the product relationship between two irreps in D_{2h} is given. Figures 5(b)–5(d) present three different electronic configuration diagrams of BeH$_2$. In Fig. 5(b) we present the Hartree-Fock ground state, i.e., the reference state, in which the three lowest orbitals with the irreps of a_g, b_{1u}, and a_g are doubly occupied. By referring to the product table in Fig. 5(a), the irrep of the reference state is easily obtained as $(a_g\otimes a_g)\otimes(b_{1u}\otimes b_{1u})\otimes(a_g\otimes a_g) = a_g\otimes a_g\otimes a_g = A_g$. Usually, the irrep of the molecular wavefunction is written in uppercase to distinguish from the irrep of the molecular orbitals. In our method, after determining the irrep of the reference state, then all the possible single Slater-determinant excited terms $\hat{t}|\Psi_0\rangle$ are traversed to check whether they share the same irrep as the reference term. We present two specific examples in Figs. 5(c) and 5(d). For the single excitation term $\hat{t}_3^4|\Psi_0\rangle$ in Fig. 5(c), one electron is excited from the third orbital to the fourth orbital. Its corresponding irrep is $(a_g\otimes a_g)\otimes(a_g\otimes a_g)\otimes(b_{1u})\otimes(b_{2u}) = a_g\otimes a_g\otimes b_{1u}\otimes b_{2u} = B_{3g} \neq A_g$, which is not expected, and the exciting operator $\hat{t}_3^4$ should be excluded from constructing the cluster operator. As shown in Fig. 5(d), both electrons at the third orbital are excited to the fourth orbital. The irrep is similarly evaluated as $(a_g\otimes a_g)\otimes(b_{1u}\otimes b_{1u})\otimes(b_{2u}\otimes b_{2u}) = a_g\otimes a_g\otimes a_g = A_g$, which is the same as the reference term. So the exciting operator $\hat{t}_{33}^{44}$ remains in constructing the cluster operator.

In total, there are 12 (3×4) single excited states and 78 double excited states for BeH$_2$. Only 23 excitations share the same irreducible representation A_g as the reference state. Thus, only the certain 23 excitation operators are included when constructing the ansatz in the following VQE steps.

APPENDIX B: VALIDATION OF THE POINT-GROUP SYMMETRY REDUCTION IN UCC

Here we give a short derivation to validate the algorithm. In the UCC theory, the wavefunction of a chemical system, $|\Psi\rangle$, is constructed from the reference wavefunction $|\Psi_0\rangle$, which is usually a Hartree-Fock Slater determinant, by applying $e^{\hat{T}-\hat{T}^\dagger}$ as

$$|\Psi\rangle = e^{\hat{T}-\hat{T}^\dagger}|\Psi_0\rangle, \tag{B1}$$

and the Schrödinger equation can be written as

$$\hat{H}|\Psi\rangle = E_{ucc}|\Psi\rangle. \tag{B2}$$

For ensuring $|\Psi\rangle$ to be a solution of the Schrödinger equation, the cluster operator $e^{\hat{T}-\hat{T}^\dagger}$ here is not arbitrary but has to

satisfy some conditions. In the following we will present how to reduce the number of operators and terms in the unitary coupled-cluster wavefunction $|\Psi\rangle$. Note that the wavefunction here refers to a solution of the Schrödinger equation instead of a quantum state prepared on a quantum computer.

Here we have assumed that both $|\Psi_0\rangle$ and $|\Psi\rangle$ are nondegenerate states. For a symmetry operation $\hat{R}_i$ belongs to an Abelian point group G, and the Hamiltonian commutes with it, $\hat{H}\hat{R}_i = \hat{R}_i\hat{H}$. Thus we have

$$\hat{H}\hat{R}_i|\Psi\rangle = \hat{R}_i\hat{H}|\Psi\rangle = E_{ucc}\hat{R}_i|\Psi\rangle = E_{ucc}(\hat{R}_i|\Psi\rangle). \tag{B3}$$

It indicates that $\hat{R}_i|\Psi\rangle$ is also the eigenstate of the Hamiltonian. So we come to

$$\exists\gamma : \hat{R}_i|\Psi\rangle = \gamma|\Psi\rangle, \tag{B4}$$

where the value of γ is the irreducible character that can be looked up from the character table of the corresponding point group. The irreducible characters in the Abelian point group are always 1 or -1.

In the following, we will show that $|\Psi_0\rangle$ and $|\Psi\rangle$ belong to the same irrep:

$$D(|\Psi_0\rangle) = D(|\Psi\rangle), \tag{B5}$$

where D is the irrep of the corresponding wavefunction.

By applying the symmetry operator to $|\Psi_0\rangle$ and $|\Psi\rangle$, respectively, we have

$$\langle\Psi_0 \mid \Psi\rangle = \langle\Psi_0|R^\dagger R|\Psi\rangle = c_0 c_1 \langle\Psi_0 \mid \Psi\rangle. \tag{B6}$$

We note that a reasonable solution $|\Psi\rangle$ perturbed from $|\Psi_0\rangle$ should be overlapping with the Hartree-Fock determinant $|\Psi_0\rangle$ [77]:

$$\langle\Psi_0 \mid \Psi\rangle \neq 0. \tag{B7}$$

It indicates that

$$c_0 c = 1. \tag{B8}$$

In an Abelian point group, the characters are either 1 or -1. So we know

$$c_0 = c. \tag{B9}$$

It means that

$$\forall\hat{R}_i \in G : \hat{R}_i|\Psi_0\rangle = c_i|\Psi_0\rangle, \hat{R}_i|\Psi\rangle = c_i|\Psi\rangle. \tag{B10}$$

This concludes that each symmetry operation $\hat{R}_i \in G$ acting on $|\Psi\rangle$ and $|\Psi_0\rangle$ will lead to the same character, and thus they belong to the same irrep.

The cluster operator $e^{\hat{T}-\hat{T}^\dagger}$ might be expanded by Taylor expansion,

$$e^{\hat{T}-\hat{T}^\dagger} = 1 + (\hat{T} - \hat{T}^\dagger) + \frac{1}{2!}(\hat{T} - \hat{T}^\dagger) + \cdots. \tag{B11}$$

Thus $|\Psi\rangle$ can be written as the linear combination of Slater determinants:

$$|\Psi\rangle = k(|\Psi_0\rangle + \sum_{i,a} c_i^a|\Psi_i^a\rangle + \sum_{i,j,a,b} c_{ij}^{ab}|\Psi_{ij}^{ab}\rangle + \cdots), \tag{B12}$$

where k is the normalized coefficient and c is the summarized coefficient of each excited term including connected and disconnected terms.

As we have presented that the $|\Psi\rangle$ and $|\Psi_0\rangle$ are of the same irrep, so all the terms in the expansion are required to have the same irrep as the reference wavefunction. If $D(c_i^a|\Psi_i^a\rangle) \neq D(|\Psi_0\rangle)$, $c_i^a|\Psi_i^a\rangle$ must be *zero*.

It indicates that only the excitation and deexcitation operators, $\hat{t}$ and $\hat{t}^\dagger$, belonging to the corresponding irrep can survive. Otherwise, the excited term $|\Psi_k\rangle$ belonging to another irrep would appear in the expansion of $|\Psi\rangle$. So in our algorithm, we filter out the excitation (and the deexcitation) operators belong to the different irreps:

$$\forall D(\hat{t}|\Psi_0\rangle) \neq D(|\Psi_0\rangle) : \hat{t} = 0. \tag{B13}$$

Considering the ansatz after Trotterization, it can alternatively be stated as

$$\forall D(e^{\hat{t}-\hat{t}^\dagger}|\Psi_0\rangle) \neq D(|\Psi_0\rangle) : e^{\hat{t}-\hat{t}^\dagger} = 1. \tag{B14}$$

When applying this method, it is implicitly assumed that the irrep of the Hartree-Fock reference state is of the correct irrep of the true ground state. We will discuss how this assumption might affect the application of the proposed algorithm. For the simple closed-shell molecules like BeH_2 (meaning there is no unpaired electron), the ground state is necessarily of the totally symmetric irrep, such as A_g in the D_{2h} group, A_1 in the C_{2v} group, and A' in the C_s group. This conclusion applies to most of the organic compounds and simple ionic compounds

including all the cases listed in this work [74]. However, when it comes to molecules with unpaired electrons, the irrep of the ground state cannot get determined directly. In such situations, the ground state evaluated by Hartree-Fock is a good starting point and usually predicts the correct irrep of the true ground state. For more complex cases where a single Slater determinant is not a good approximation, multiple attempts of the Hartree-Fock ground state and low-lying excited states may be needed for reaching the true ground state, as what has been done in conventional quantum chemical calculations.

APPENDIX C: PARAMETERS COUNTING AND REDUCTION

The wavefunction $|\Psi\rangle$ constructed from the UCCSD ansatz $|\Psi\rangle = e^{\hat{T}-\hat{T}^\dagger}|\Psi_0\rangle$ is actually implemented by fermion-spin transformations (such as Jordan-Wigner transformation and Bravyi-Kitaev transformation) and first-order Trotterization. After that, the quantum circuit can be treated as the product of a series of time evolution of Pauli strings like $U(\vec{\theta}) = e^{i\theta_1\hat{P}_1}e^{i\theta_2\hat{P}_2}e^{i\theta_3\hat{P}_3}\cdots$, where $\hat{P}_i$ are Pauli strings.

For example, if the variational parameter θ is real, after Jordan-Wigner transformation, the single excitation operators become

$$\hat{t}_i^a - \hat{t}_i^{a\dagger} = \theta_i^a(a_a^\dagger a_i - a_i^\dagger a_a)$$

$$= \frac{\theta_i^a}{4}\left[(\sigma_a^x - i\sigma_a^y)(-\sigma_i^x + i\sigma_i^y) - (\sigma_i^x - i\sigma_i^y)(-\sigma_a^x + i\sigma_a^y)\right]\left(\bigotimes_{k=i+1}^{a-1}\sigma_k^z\right)$$

$$= i\frac{\theta_i^a}{2}\left(\sigma_a^y\sigma_i^x - \sigma_a^x\sigma_i^y\right)\left(\bigotimes_{k=i+1}^{a-1}\sigma_k^z\right), \tag{C1}$$

$[\sigma_a^y\sigma_i^x, \sigma_m^x\sigma_n^y] = 0$ if $m \neq a$, $n \neq i$. After first-order Trotterization, the unitary operators may looks like $e^{i\frac{\theta_i^a}{2}\sigma_a^y\sigma_k^z\cdots\sigma_i^x}$, $e^{i\frac{\theta_i^a}{2}\sigma_a^x\sigma_k^z\cdots\sigma_i^y}$, etc. Similarly, the double excitation operators will become

$$\hat{t}_{ij}^{ab} - \hat{t}_{ij}^{ab\dagger} = \theta_{ij}^{ab}(a_a^\dagger a_b^\dagger a_i a_j - a_j^\dagger a_i^\dagger a_b a_a)$$

$$= \frac{\theta_{ij}^{ab}}{16}\left[(\sigma_a^x - i\sigma_a^y)(\sigma_b^x + i\sigma_b^y)(\sigma_i^x + i\sigma_i^y)(-\sigma_j^x + i\sigma_j^y) - (\sigma_a^x + i\sigma_a^y)(-\sigma_b^x + i\sigma_b^y)(\sigma_i^x - i\sigma_i^y)(\sigma_j^x + i\sigma_j^y)\right]$$

$$\times \left(\bigotimes_{k=m+1}^{i-1}\sigma_k^z\right)\left(\bigotimes_{p=n+1}^{j-1}\sigma_p^z\right)$$

$$= \frac{\theta_{ij}^{ab}}{8}\left(i\sigma_a^y\sigma_b^x\sigma_i^x\sigma_j^x - i\sigma_a^x\sigma_b^y\sigma_i^x\sigma_j^x - i\sigma_a^x\sigma_b^x\sigma_i^y\sigma_j^x + i\sigma_a^x\sigma_b^x\sigma_i^x\sigma_j^y - i\sigma_a^y\sigma_b^y\sigma_i^y\sigma_j^x + i\sigma_a^y\sigma_b^y\sigma_i^x\sigma_j^y\right.$$

$$\left. + i\sigma_a^y\sigma_b^x\sigma_i^y\sigma_j^y - i\sigma_a^x\sigma_b^y\sigma_i^y\sigma_j^y\right)\left(\bigotimes_{k=m+1}^{i-1}\sigma_k^z\right)\left(\bigotimes_{p=n+1}^{j-1}\sigma_p^z\right), \tag{C2}$$

and there will be a similar time evolution of Pauli strings after Trotterization.

To realize the time evolution of Pauli strings, for instance, the operator $e^{i\theta\sigma_1^z\sigma_2^z\sigma_3^z\sigma_4^z}$ may be decomposed into single-qubit rotation gates and a two-qubit controlled-NOT (CNOT) gate [78] as
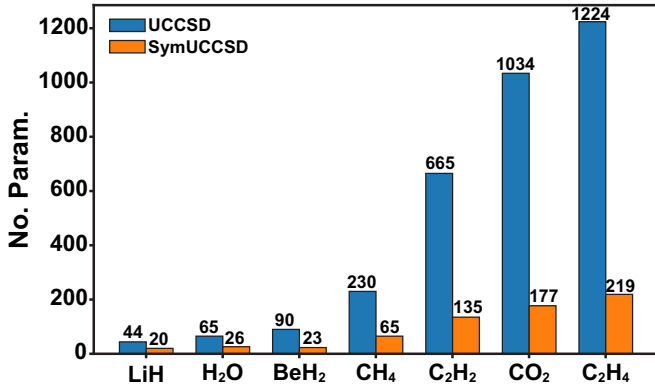

$$\tag{C3}$$
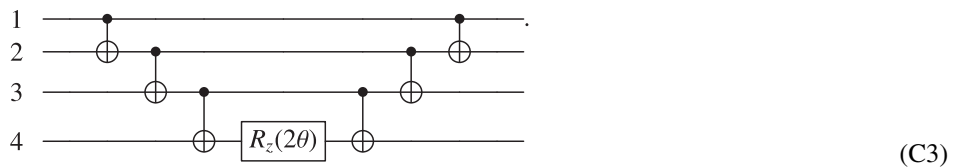
FIG. 8. The number of parameters for a series of molecules before and after the reduction by point-group symmetry. We observed that the ratio of the necessary parameters decreases slightly as the size of the system increases, ranging from 25.6% of BeH_2, to 20.3% of C_2H_2, and to 17.9% of C_2H_4, all of which are of the same D_{2h} symmetry, indicating better efficiency for larger molecules.

Other operators may be decomposed to similar circuits other than some single rotations. According to the point-group constraint, the symmetry-forbidden $e^{\hat{t}-\hat{t}^\dagger}$ will be eliminated and the corresponding Pauli strings in the quantum circuit will disappear, leading to significant reduction in the circuit depth.

In this work, we use the number of parameters (equal to the number of excitation operators) to measure the compactness of the ansatz. Considering a restricted closed-shell molecule with n occupied spatial orbitals and m virtual spatial orbitals, the number of parameters is counted in the following principles:

(1) For the single excitation, the number of possible excitation operators is $m \times n$.

(2) For the double excitation, the number of possible excitation operators is computed by the pair excitation $\hat{t}_{ii}^{aa}$ with $m \times n$ terms plus the direct product of the two different single excitations with $C_{mn}^2 = m \times n(m \times n - 1)/2$ terms.

We apply this method to a series of molecules (without further VQE steps) and compare parameter numbers in the ansatz before and after symmetry reduction in Fig. 8. The number of the parameters grows much slower after filtering out the symmetry-forbidden terms, indicating a shallower quantum circuit and a smaller need for computational resources.

APPENDIX D: SYMUCCSD COMPARED AND COMBINED WITH ADAPT-VQE

The point group employed in SymUCCSD can compare and combine with an adaptive-type ansatz. One of the famous adaptive variational quantum eigensolvers is ADAPT-VQE proposed in Ref. [20]. ADAPT-VQE screens operators from a predefined pool to construct the circuit of ansatz, and the operator that will result in a larger gradient to the energy would be chosen. In ADAPT-VQE, the operator pool is composed of a set of spin-adapted single and double excitation operators. The screening step is terminated when the average gradient of the operators is smaller than the predefined threshold ϵ.

In this section, we present the results of ADAPT-VQE [20] as both comparison of and in combination with SymUCCSD. The calculations are performed using the MindQuantum simulator [45] with STO-3G basis set [46], and the ϵ is set to 10^{-2}.

As shown in Table III, we have performed a series of ADAPT-VQE calculations with different initial operator pools. First, as a comparison in the second and seventh rows of Table III, we observe that SymUCCSD reaches similar accuracy with slightly more parameters (23 parameters compared to 18 parameters), when compared with ADAPT-VQE. However, SymUCCSD does not need to evaluate the gradient of each operator on quantum computers, the evaluation of which will be extra measurement overhead on real quantum devices.

Besides, we also try to combine SymUCCSD with the ADAPT-VQE method. As shown in the second row of Table III, we initialize the operator pool of ADAPT-VQE based on the point-group symmetry. The number of operators is reduced from 90 to 23 as what has been done in SymUCCSD. By taking this reduced initial operator pool, the number of final operators and energy are the same as those using the default full operator pool.

To get more insights from ADAPT-VQE and point-group symmetry, we further carried out two ADAPT-VQE calculations as shown in Table III, rows 4 and 7. Both of the calculations fail with the these initial operator pools. For

TABLE III. Numerical simulations of ADAPT-VQE ($\epsilon = 0.01$) and SymUCCSD methods. The size of the initial and final operator pool is listed in the first and second columns. The energy with respect to FCI energy is given in the fourth column. The Hartree-Fock, CCSD, and FCI energies calculated using the PySCF [43,44] package and SymUCCSD energy are calculated using the method as mentioned in the paper.

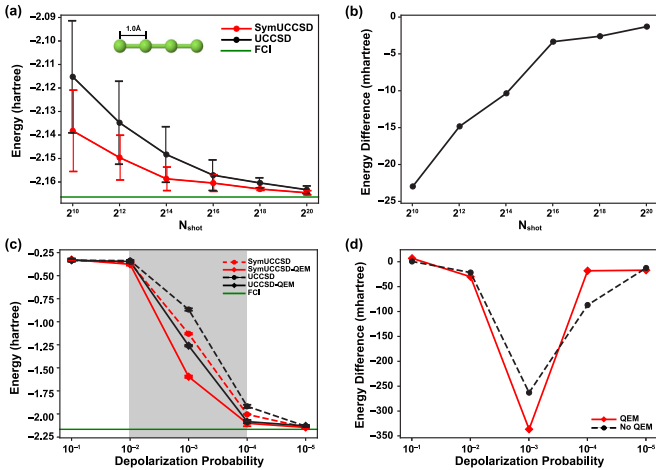| Method	Initial operators	Final operators	Energy/hartree	ΔE/mhartree
ADAPT-VQE	90 (Origin)	18	−15.5948	0.4
ADAPT-VQE	23 (Same irrep)	18	−15.5948	0.4
ADAPT-VQE	23 (Random)	5	−15.5608	34.4
ADAPT-VQE	67 (Different irrep)	0	−15.5603	34.9
UCCSD	90	90	−15.5948	0.4
SymUCCSD	23	23	−15.5948	0.4
Hartree-Fock			−15.5603	34.9
CCSD			−15.5948	0.4
FCI			−15.5952	0

FIG. 9. The numerical simulation of an H_4 molecule with uncertainties. (a) The energy vs the number of shots without introducing noise model. (b) The difference between energies calculated by SymUCCSD and UCCSD ansatzes. (c) The energy vs the depolarization probability. The depolarizing noise model provided by QISKIT [79] is used. The quantum error mitigation (QEM) is performed using zero-noise extrapolation based on a linear fit implemented with the MITIQ [80] package. The magnitude of the standard deviation is tens of millihartree, which makes the error bar look narrow due to the large scaling of the *y* axis. (d) The difference between energies calculated by SymUCCSD and UCCSD ansatzes.

the initial operator pools with 23 randomly selected operators, the algorithm only chooses 5 operators in the final, and the final energy is far from the energy calculated from FCI or CCSD. While for the initial operator pool with 67 operators, none of the operators survives in the ADAPT-VQE process and the Hartree-Fock level energy is obtained. These results indicate that the valid operators in ADAPT-VQE indeed conserve the point-group symmetry.

In summary, the point-group symmetry reduction in SymUCCSD not only efficiently saves computational

resources on its own, but it is also compatible with other methods such as ADAPT-VQE to further reduce quantum resource requirements (here meaning extra quantum measurement overhead).

APPENDIX E: NUMERICAL SIMULATIONS WITH NOISE AND MEASUREMENT SHOTS

To assess the performance of the SymUCCSD on a real quantum device, we evaluate the influence introduced by imperfect device noise and number of measurement shots. We compare SymUCCSD and UCCSD ansatzes for an eight-qubit system of an H_4 chain with equal space ($r = 1$ Å) using the STO-3G basis set [46] and carry out the numerical simulation using the Qiskit toolkit with QASM simulator with and without noise models [79].

In Fig. 9(a), we show the VQE energy without any noise. The energy decreases as the number of shots increases. We observed that the energy of SymUCCSD converges faster and has smaller fluctuation than that of UCCSD with the increasing of measurement shots. This relative fluctuation in UCCSD is mainly because of the very small part of the computational-basis state out of the desired irrep. The energy differences between SymUCCSD and UCCSD reach ~1 millihartree at the large number of shots 2^{20}, as shown in Fig. 9(b).

In Figs. 9(c) and 9(d), we consider the effect of noise by introducing the depolarizing noise model. The quantum error mitigation (QEM) is performed using zero-noise extrapolation based on a linear fit implemented by the MITIQ package [80]. We observed the SymUCCSD ansatz is more robust to noise (particularly in the range of 10^{-2} to 10^{-3}, which is the current state of the art for real quantum devices) in situations both with and without error mitigation, respectively, which is understandable since SymUCCSD has much shallower circuits.

In a word, with the help of the point-group symmetry reduction, we can construct a more compact ansatz SymUCCSD with less parameters. It may not only reduce the computational cost but also provide better accuracy on real quantum devices.

[1] R. P. Feynman, Int. J. Theor. Phys. **21**, 467 (1982).

[2] A. Aspuru-Guzik, A. D. Dutoi, P. J. Love, and M. Head-Gordon, Science **309**, 1704 (2005).

[3] I. Kassal, S. P. Jordan, P. J. Love, M. Mohseni, and A. Aspuru-Guzik, Proc. Natl. Acad. Sci. USA **105**, 18681 (2008).

[4] J. Huh, G. G. Guerreschi, B. Peropadre, J. R. Mcclean, and A. Aspuru-Guzik, Nat. Photonics **9**, 615 (2015).

[5] S. McArdle, S. Endo, A. Aspuru-Guzik, S. C. Benjamin, and X. Yuan, Rev. Mod. Phys. **92**, 015003 (2020).

[6] R. Babbush, N. Wiebe, J. McClean, J. McClain, H. Neven, and G. K.-L. Chan, Phys. Rev. X **8**, 011044 (2018).

[7] P. Zeng, J. Sun, and X. Yuan, arXiv:2109.15304.

[8] A. Peruzzo, J. McClean, P. Shadbolt, M.-H. Yung, X.-Q. Zhou, P. J. Love, A. Aspuru-Guzik, and J. L. O'Brien, Nat. Commun. **5**, 4213 (2014).

[9] M.-H. Yung, J. Casanova, A. Mezzacapo, J. McClean, L. Lamata, A. Aspuru-Guzik, and E. Solano, Sci. Rep. **4**, 3589 (2015).

[10] S. Endo, J. Sun, Y. Li, S. C. Benjamin, and X. Yuan, Phys. Rev. Lett. **125**, 010501 (2020).

[11] A. Kandala, A. Mezzacapo, K. Temme, M. Takita, M. Brink, J. M. Chow, and J. M. Gambetta, Nature (London) **549**, 242 (2017).

[12] X. Xu, J. Sun, S. Endo, Y. Li, S. C. Benjamin, and X. Yuan, Sci. Bull. **66**, 2181 (2021).

[13] P. J. J. O'Malley, R. Babbush, I. D. Kivlichan, J. Romero, J. R. McClean, R. Barends, J. Kelly, P. Roushan, A. Tranter, N. Ding *et al.*, Phys. Rev. X **6**, 031007 (2016).

[14] Y. Nam, J.-S. Chen, N. C. Pisenti, K. Wright, C. Delaney, D. Maslov, K. R. Brown, S. Allen, J. M. Amini, J. Apisdorf *et al.*, npj Quantum Inf. **6**, 33 (2020).

[15] F. Arute, K. Arya, R. Babbush, D. Bacon, J. C. Bardin, R. Barends, S. Boixo, M. Broughton, B. B. Buckley, D. A. Buell *et al.*, Science **369**, 1084 (2020).

[16] K. Yeter-Aydeniz, B. T. Gard, J. Jakowski, S. Majumder, G. S. Barron, G. Siopsis, T. S. Humble, and R. C. Pooser, Adv. Quantum Technol. **4**, 2100012 (2021).

[17] P. Lolur, M. Rahm, M. Skogh, L. García-Álvarez, and G. Wendin, AIP Conf. Proc. **2362**, 030005 (2021).

[18] M. Kühn, S. Zanker, P. Deglmann, M. Marthaler, and H. Weiß, J. Chem. Theory Comput. **15**, 4764 (2019).

[19] Y. Wu, W.-S. Bao, S. Cao, F. Chen, M.-C. Chen, X. Chen, T.-H. Chung, H. Deng, Y. Du, D. Fan *et al.*, Phys. Rev. Lett. **127**, 180501 (2021).

[20] H. R. Grimsley, S. E. Economou, E. Barnes, and N. J. Mayhall, Nat. Commun. **10**, 3007 (2019).

[21] J. Romero, R. Babbush, J. R. McClean, C. Hempel, P. J. Love, and A. Aspuru-Guzik, Quantum Sci. Technol. **4**, 014008 (2018).

[22] Y. Fan, C. Cao, X. Xu, Z. Li, D. Lv, and M.-H. Yung, arXiv:2106.15210.

[23] D. Wecker, M. B. Hastings, and M. Troyer, Phys. Rev. A **92**, 042303 (2015).

[24] I. G. Ryabinkin, T.-C. Yen, S. N. Genin, and A. F. Izmaylov, J. Chem. Theory Comput. **14**, 6317 (2018).

[25] I. G. Ryabinkin, R. A. Lang, S. N. Genin, and A. F. Izmaylov, J. Chem. Theory Comput. **16**, 1055 (2020).

[26] P. L. Dallaire-Demers, J. Romero, L. Veis, S. Sim, and A. Aspuru-Guzik, Quantum Sci. Technol. **4**, 045005 (2019).

[27] J. Lee, W. J. Huggins, M. Head-Gordon, and K. B. Whaley, J. Chem. Theory Comput. **15**, 311 (2019).

[28] S. Bravyi, J. M. Gambetta, A. Mezzacapo, and K. Temme, arXiv:1701.08213.

[29] B. T. Gard, L. Zhu, G. S. Barron, N. J. Mayhall, S. E. Economou, and E. Barnes, npj Quantum Inf. **6**, 10 (2020), 1904.10910.

[30] G. Greene-Diniz and D. Muñoz Ramo, Int. J. Quantum Chem. **121**, e26352 (2021).

[31] P. Čársky, Jr., L. J. Schaad, B. A. Hess, M. Urban, and J. Noga, J. Chem. Phys. **87**, 411 (1987).

[32] J. F. Stanton, J. Gauss, J. D. Watts, and R. J. Bartlett, J. Chem. Phys. **94**, 4334 (1991).

[33] G. E. Scuseria, A. C. Scheiner, T. J. Lee, J. E. Rice, and H. F. Schaefer, J. Chem. Phys. **86**, 2881 (1987).

[34] K. Setia, R. Chen, J. E. Rice, A. Mezzacapo, M. Pistoia, and J. D. Whitfield, J. Chem. Theory Comput. **16**, 6091 (2020).

[35] S. A. Fischer and D. Gunlycke, arXiv:1907.01493.

[36] K. Seki, T. Shirakawa, and S. Yunoki, Phys. Rev. A **101**, 052340 (2020).

[37] T.-C. Yen, R. A. Lang, and A. F. Izmaylov, J. Chem. Phys. **151**, 164111 (2019).

[38] M. R. Hoffmann and J. Simons, J. Chem. Phys. **88**, 993 (1988).

[39] R. J. Bartlett, S. A. Kucharski, and J. Noga, Chem. Phys. Lett. **155**, 133 (1989).

[40] Y. Shen, X. Zhang, S. Zhang, J.-N. Zhang, M.-H. Yung, and K. Kim, Phys. Rev. A **95**, 020501(R) (2017).

[41] J. Liu, J. Sun, and X. Yuan, arXiv:2109.05547.

[42] P. K. Barkoutsos, J. F. Gonthier, I. Sokolov, N. Moll, G. Salis, A. Fuhrer, M. Ganzhorn, D. J. Egger, M. Troyer, A. Mezzacapo, S. Filipp, and I. Tavernelli, Phys. Rev. A **98**, 022322 (2018).

[43] Q. Sun, X. Zhang, S. Banerjee, P. Bao, M. Barbry, N. S. Blunt, N. A. Bogdanov, X. Wang, A. White, J. D. Whitfield *et al.*, J. Chem. Phys. **153**, 024109 (2020).

[44] Q. Sun, T. C. Berkelbach, N. S. Blunt, G. H. Booth, S. Guo, Z. Li, J. Liu, J. D. McClain, E. R. Sayfutyarova, S. Sharma, S. Wouters, and G. K.-L. Chan, WIREs Comput. Mol. Sci. **8**, e1340 (2018).

[45] Huawei, Mindquantum (2021), https://gitee.com/mindspore/mindquantum.

[46] W. J. Hehre, R. Ditchfield, R. F. Stewart, and J. A. Pople, J. Chem. Phys. **52**, 2769 (1970).

[47] P. Jordan and E. P. Wigner, Z. Physik **47**, 631 (1928).

[48] N. Russell Johnson, NIST computational chemistry comparison and benchmark database (2020).

[49] J. P. Perdew, K. Burke, and M. Ernzerhof, Phys. Rev. Lett. **77**, 3865 (1996).

[50] F. Weigend and R. Ahlrichs, Phys. Chem. Chem. Phys. **7**, 3297 (2005).

[51] Z. Holmes, K. Sharma, M. Cerezo, and P. J. Coles, PRX Quantum **3**, 010313 (2022).

[52] M. Larocca, N. Ju, D. García-Martín, P. J. Coles, and M. Cerezo, arXiv:2109.11676.

[53] M. Motta, E. Ye, J. R. McClean, Z. Li, A. J. Minnich, R. Babbush, and G. K.-L. Chan, npj Quantum Inf. **7**, 83 (2021).

[54] Y. Matsuzawa and Y. Kurashige, J. Chem. Theory Comput. **16**, 944 (2020).

[55] N. C. Rubin, J. Lee, and R. Babbush, J. Chem. Theory Comput. **18**, 1480 (2022).

[56] J. S. Kottmann and A. Aspuru-Guzik, Phys. Rev. A **105**, 032449 (2022).

[57] H. L. Tang, V. O. Shkolnikov, G. S. Barron, H. R. Grimsley, N. J. Mayhall, E. Barnes, and S. E. Economou, PRX Quantum **2**, 020310 (2021).

[58] Z.-J. Zhang, J. Sun, X. Yuan, and M.-H. Yung, arXiv:2011.05283.

[59] C. J. Trout and K. R. Brown, Int. J. Quantum Chem. **115**, 1296 (2015).

[60] T. Jones and S. C. Benjamin, Quantum **6**, 628 (2022).

[61] J. Sun, S. Endo, H. Lin, P. Hayden, V. Vedral, and X. Yuan, arXiv:2106.05938.

[62] K. Fujii, K. Mitarai, W. Mizukami, and Y. O. Nakagawa, PRX Quantum **3**, 010346 (2022).

[63] K. Mizuta, M. Fujii, S. Fujii, K. Ichikawa, Y. Imamura, Y. Okuno, and Y. O. Nakagawa, Phys. Rev. Research **3**, 043121 (2021).

[64] T. Takeshita, N. C. Rubin, Z. Jiang, E. Lee, R. Babbush, and J. R. McClean, Phys. Rev. X **10**, 011004 (2020).

[65] X. Yuan, J. Sun, J. Liu, Q. Zhao, and Y. Zhou, Phys. Rev. Lett. **127**, 040501 (2021).

[66] G. Knizia and G. K.-L. Chan, Phys. Rev. Lett. **109**, 186404 (2012).

[67] N. C. Rubin, arXiv:1610.06910.

[68] Y. Kawashima, M. P. Coons, Y. Nam, E. Lloyd, S. Matsuura, A. J. Garza, S. Johri, L. Huntington, V. Senicourt, A. O. Maksymov *et al.*, Commun. Phys. **4**, 245 (2021).

[69] L. Mineh and A. Montanaro, Phys. Rev. B **105**, 125117 (2022).

[70] W. Li, Z. Huang, C. Cao, Y. Huang, Z. Shuai, X. Sun, J. Sun, X. Yuan, and D. Lv, arXiv:2109.08062.

[71] G. Kotliar, S. Y. Savrasov, K. Haule, V. S. Oudovenko, O. Parcollet, and C. A. Marianetti, Rev. Mod. Phys. **78**, 865 (2006).

[72] B. Bauer, D. Wecker, A. J. Millis, M. B. Hastings, and M. Troyer, Phys. Rev. X **6**, 031045 (2016).

[73] I. Rungger, N. Fitzpatrick, H. Chen, C. Alderete, H. Apel, A. Cowtan, A. Patterson, D. M. Ramo, Y. Zhu, N. H. Nguyen *et al.*, arXiv:1910.04735.

[74] F. A. Cotton, *Chemical Applications of Group Theory* (Wiley, New York, 2003).

[75] R. Mirman, *Point Groups, Space Groups, Crystals, Molecules* (World Scientific, Singapore, 1999).

[76] P. H. Butler, *Point Group Symmetry Applications: Methods and Tables* (Springer, Berling, 2012).

[77] A. G. Taube and R. J. Bartlett, Int. J. Quantum Chem. **106**, 3393 (2006).

[78] M. A. Nielsen and I. Chuang, Am. J. Phys. **70**, 558 (2002).

[79] M. S. Anis, H. Abraham *et al.*, Qiskit: An open-source framework for quantum computing (2021).

[80] R. LaRose, A. Mari, S. Kaiser, P. J. Karalekas, A. A. Alves, P. Czarnik, M. E. Mandouh, M. H. Gordon, Y. Hindy, A. Robertson, P. Thakre, N. Shammah, and W. J. Zeng, arXiv:2009.04417.